

# Exploring DHCAL design and performance with Graph Neural Networks

---

**M. Borysova,<sup>1</sup> D. Zavazieva,<sup>1,2</sup> N. Kakati,<sup>1</sup> E. Gross<sup>1</sup> and S. Bressler<sup>1</sup>**

<sup>1</sup>*Weizmann Institute of Science, Rehovot, Israel*

<sup>2</sup>*Ben-Gurion University of the Negev, Be'er Sheva, Israel*

*E-mail:* [maryna.borysova@weizmann.ac.il](mailto:maryna.borysova@weizmann.ac.il)

**ABSTRACT:** In the context of a gas-sampling Digital Hadronic Calorimeter (DHCAL), we explore the potential of using Graph Neural Networks (GNNs) for hadron energy reconstruction and particle identification (PID) in future collider experiments. For PID, we achieve a classification efficiency of  $\sim 90\%$  for neutrons and pions, and nearly  $100\%$  for neutral kaons and protons. The energy resolution for these hadrons is studied in the energy range of  $1 - 50$  GeV, with a further investigation into the resolution as a function of the incoming particle's angle and readout granularity, focusing on charged pions. Compared to traditional analysis methods, our results indicate that improved performance can be achieved even with coarser detector granularity, potentially making future DHCAL systems more cost-effective.

**KEYWORDS:** HCAL, DHCAL, RPC, RPWELL, GNN, ML, PID, Energy resolution

**ARXIV EPRINT:** [2501.00128](https://arxiv.org/abs/2501.00128)

---

<sup>1</sup>Corresponding author.

---

## Contents

<b>1</b>	<b>Introduction</b>	<b>1</b>
<b>2</b>	<b>Methods</b>	<b>3</b>
2.1	GEANT4 simulation	3
2.2	Neural Networks	4
2.3	Particle Identification (PID) and energy reconstruction	5
2.3.1	The Neural Network (NN) prediction	5
2.3.2	Performance quantification	6
<b>3</b>	<b>Results</b>	<b>7</b>
3.1	Particle Identification	7
3.2	Energy reconstruction	9
3.3	Different detector performance and design	11
<b>4</b>	<b>Discussion</b>	<b>12</b>

---

## 1 Introduction

Machine Learning (ML) has made a profound impact on physics research, particularly in particle physics, where it has been successfully applied to a wide range of tasks, including data collection, physics object reconstruction, and PID. In particle physics, accurate jet measurement is essential for understanding the fundamental properties of particles and their interactions. Therefore, the Hadronic Calorimeter (HCAL) in future collider facilities requires exceptional hadron energy resolution, with the goal of achieving  $\frac{\Delta E}{E} \leq 55\%$  [1]. Despite advancements, precision measurement of hadronic showers remains a significant challenge. When hadrons interact with a calorimeter, a diverse array of nuclear processes can occur as the energy is absorbed. As demonstrated in Figure 1, this leads to substantial event-by-event fluctuations in the types and multiplicity of secondary particles, the spatial distribution of their energy deposits, and the fraction of invisible energy lost to nuclear binding energy. These factors are all dependent on the energy and type of the incident particle.

One of the most significant challenges arises from the differing responses of most HCALs to hadrons and electrons, i.e.,  $e/h$  ratio is not equal to unity [2]. This discrepancy complicates the task of directly measuring the incoming hadron energy based solely on the detected signals. This problem is enhanced due to the large event-by-event fluctuations of hadronic showers which are attributed, among others, to the energy transfer from hadronic to electromagnetic component via  $\pi_0$  production.

The energy reconstruction of these showers can be further complicated by energy leakage due to insufficient coverage of the detector or energy losses due to missing channels. Given the multidimensional challenges associated with reconstructing the energy of hadronic showers,

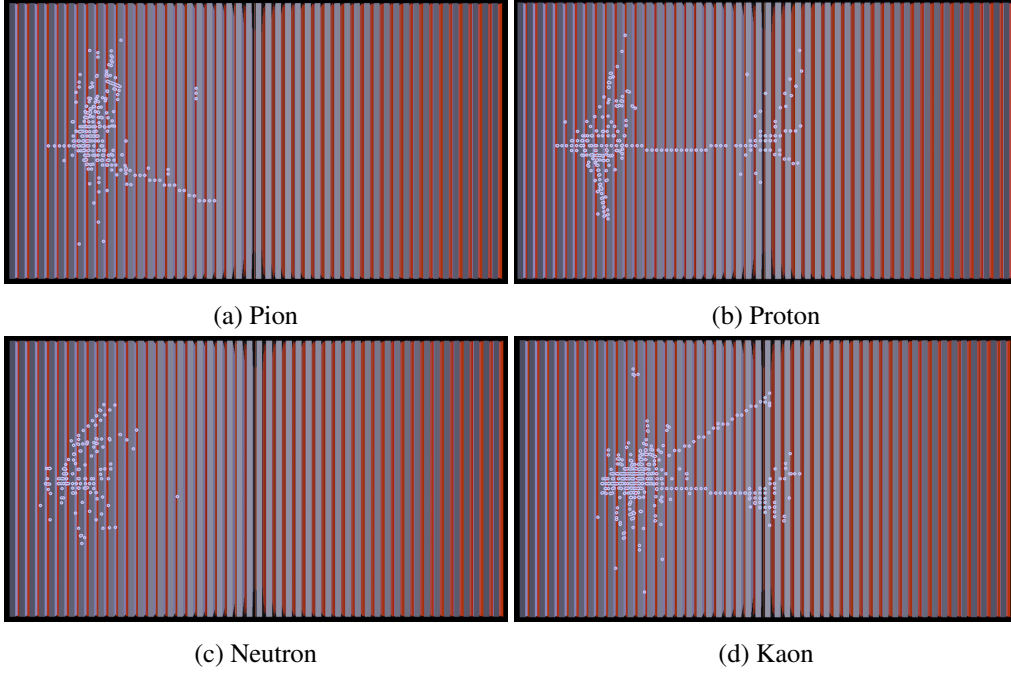


**Figure 1:** Event displays of simulated  $\pi^-$ ,  $p$ ,  $n$ ,  $K_L^0$  hadron showers. See Section 2.1 for simulation details.

traditional algorithms such as the weighted summation method [3] are often complex, require arbitrary parameterization choices, and do not fully address the aforementioned issues.

Particle Flow (PF) has emerged as a solution to address these challenges and is now the most widely used technique for reconstructing individual particles within jets in high-energy physics experiments [1]. Its goal is to measure each final-state particle within the optimal sub-detector. This requires high granularity in the calorimeters to accurately associate energy deposits with individual particles, separate nearby particle showers, and match the showers of charged particles with tracks in the tracking system.

Several high-granularity HCAL systems, which differ in their readout schemes, are considered: Analogue Hadronic Calorimeter (AHCAL), which measures both the position and the deposited energy; Semi-Digital Hadronic Calorimeter (SDHCAL), incorporating typically  $1 \times 1 \text{ cm}^2$  pads with 2-bit precision to measure the deposited energy, potentially providing information on hit multiplicity; and DHCAL, which features a simpler binary readout (hit/no-hit) for  $1 \times 1 \text{ cm}^2$  pads. The latter approach simplifies the complexity and cost of the calorimeter’s readout system, making smaller cell sizes practical for a hadron calorimeter.

Traditional Particle Flow Algorithm (PFA) methods convert the number of measured hits in the DHCAL to the energy of the incoming particle [4, 5]. More advanced algorithms also account for the hit density in different layers. ML models offer a robust approach for developing customized shower separation algorithms based on event-specific information. Currently, experiments at the CERN Large Hadron Collider (LHC) and future circular colliders utilize parameterized PFA [6] with sophisticated energy clustering algorithms [6], [7], [8] and with inclusion of timing information [9].

GNNs have emerged as an architecture of choice in recent particle reconstruction models,

demonstrating superior performance in shower separation compared to traditional convolutional neural networks for PF [10]. This success is primarily due to their ability to learn the shower shape within a given detector geometry.

ML-based reconstruction algorithms, assuming AHCALs with a highly granular scintillator medium, have been developed by the CALICE [11], CMS [12], and CEPC [13] collaborations. CALICE has also explored such algorithms for SDHCAL, using Glass Resistive Plate Chambers (RPCs) as the sensitive medium [14].

In this work, we explore the potential of GNNs to improve the design and performance of a sampling HCAL with digital (1 bit) readout, i.e., DHCAL. Building on the approach of [4], we use a GEANT4 [15] model to simulate the response of a fully equipped Resistive Plate WELL (RPWELL)-based DHCAL to pions, protons, kaons, and neutrons at a variety of energies, angles, detector designs and performances. In the following we discuss the application of GNNs to energy reconstruction and PID. The methods employed in this work are detailed in Section 2, followed by the results in Section 3. We discuss our findings in Section 4.

## 2 Methods

### 2.1 GEANT4 simulation

GEANT4<sup>1</sup> was used to model a DHCAL module and generate datasets for training and testing the performance of the NNs. The model was extensively validated with test beam data in [4]. It consists of 50 layers of RPWELL-based sampling elements and 2 cm-thick steel absorbers (Figures 2a, 2b), corresponding to a total depth of approximately  $5\lambda_\pi$ . This depth ensures a 99.3% probability that a pion will initiate a shower within the module, minimizing energy leakage. To mitigate further the effects of longitudinal leakage, we applied a pre-selection criterion, requiring the shower to initiate within the first 10 layers of the calorimeter. Depending on the simulated hadron, this condition was met by 64-67% of all simulated showers.

Sampling elements with readout pads arranged in a circular pattern, featuring varying pad sizes ranging from  $1 \times 1\text{cm}^2$  to  $4 \times 4\text{cm}^2$ , were considered to explore the sensitivity of the performance on the readout granularity. A complete anode design using  $1 \times 1\text{cm}^2$  pads is shown in Figure 2c. The energy deposits were digitized into electronic signals, emulating various pad multiplicities and hit detection efficiency values. Fired neighboring pads were grouped into clusters, with the cluster's position determined as the average of the positions of all individual pads within the cluster.

As detailed in Section 3, depending on the specific task, different datasets were generated. These include different mixtures of hadrons, their energies, and impinging angles. For each particle type, the data set, after pre-selection, contains approximately 600k events that were used for the training of the NNs, 100k events for validation and another set of 110k events, not seen by the network, for performance testing. For the angle studies, larger data sets were generated: 6M (training) and 1.5M (validating/testing) events for testing performance in the angular range of 0-40° and 1.8M, 450k for narrower ranges of angles.

---

<sup>1</sup>version 10.06.p01 [15], with QGSP-BERT-EMZ physics list

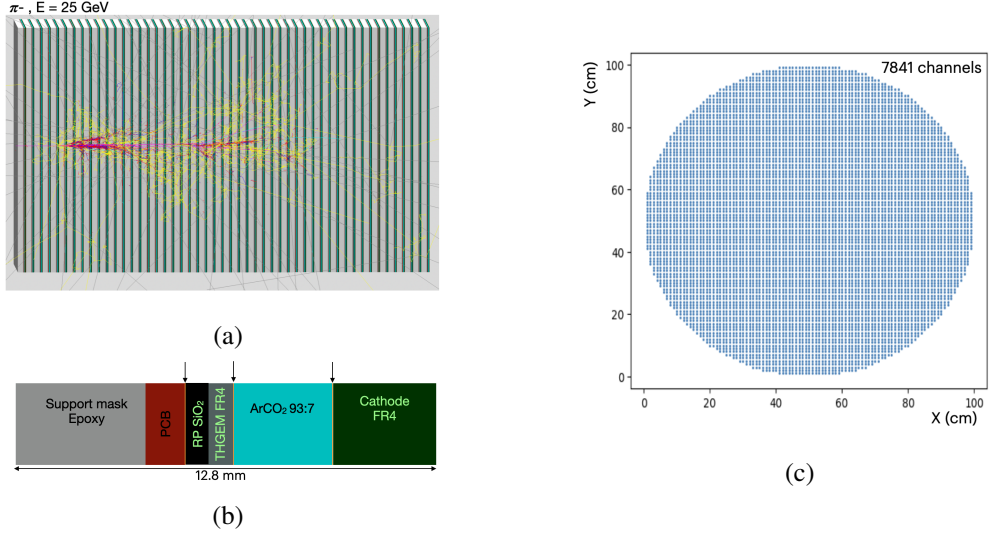


**Figure 2:** The 50 layers DHCAL GEANT4 module detailed in [4]. (a) A shower of a 25 GeV pion, excluding photons. (b) A RPWELL-based sampling element; the small arrows point from left to right on the readout anode, RPWELL to electrode, and copper cathode. (c) Readout anode with  $1 \times 1 \text{ cm}^2$  pads.

## 2.2 Neural Networks

In High Energy Physics (HEP), data is often heterogeneous and sparse, with numerous interdependencies, making graph-based algorithms a natural choice [16]. The calorimeter data under investigation is similarly sparse, with shower profiles encoded in the relationships between hits, motivating our decision to employ a graph-based representation.

While the calorimeter data can be interpreted as a 3D image, traditional image-based methods are not well-suited to address the inherent sparsity and would not generalize well to detectors with different geometries.

Relying on the graph-based approach, we represent each calorimeter cluster as a node in the graph. A collection of disconnected nodes forms a point cloud, whereas nodes connected by edges define a graph. We investigated two types of connectivity: k-nearest neighbor and radius-based methods. In this case, the latter method defines a rectangular box which connects nodes within a spatial volume of 10 clusters in all three directions. It was found to provide the most effective connectivity. The node features are characterized by the  $x$ ,  $y$ , and  $z$  coordinates of the cluster. Figure 3 illustrates two resulting graphs for a single charged pion shower: the point cloud configuration (Figure 3a) and the graph with connected nodes (Figure 3b). In addition to the individual nodes, the total number of nodes in the shower was also provided as an input to the NN.

In this study, we explored two NN architectures: one based on DeepSets [17] and the other utilizing Graph Attention Transformers (GATs) [18], [19]. Figure 4 illustrates both architectures. In each case, the input nodes, representing calorimeter clusters, are passed through a Multi-Layer Perceptron (MLP) that encodes the features into a higher-dimensional space. These cell representations are then refined through multiple iterations of either DeepSets or GATs layers.

The input to the DeepSets architecture is a point cloud. In each iteration, the nodes are

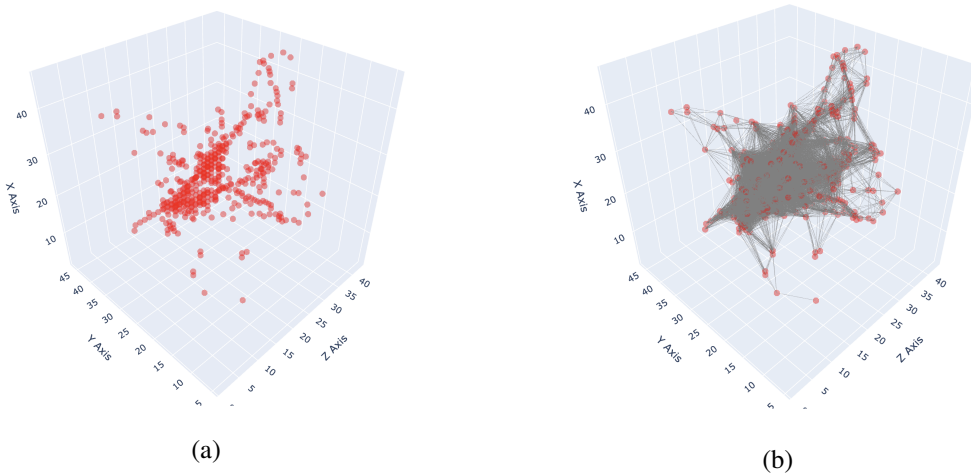


**Figure 3:** Representations of pion showers as point cloud (a) and as a graph connecting all nodes in a rectangular box spanning over a spatial volume of 10 pads in the X and Y directions and 10 layers in the Z direction (b).

aggregated using average pooling, which is then employed to update the individual cluster features. Conversely, the input to the GATs are nodes with edges (graphs). Special attention is given to the edges, allowing the GATs model to effectively exploit the underlying structure of the shower, potentially improving performance. As illustrated in Fig. 4, both architectures share a similar overall structure. The GAT model utilizes four layers, while the DeepSets architecture employs ten DeepSets layers, with these configurations chosen based on empirical performance during experimentation.

After several updates using either GATs or DeepSets, all cell representations are averaged to obtain a global representation. This global feature vector is subsequently processed through another MLP to produce the final predictions, which can either be the energy estimates or logits for classification tasks.

Both architectures were implemented in PyTorch [20], with the AdamW [21] optimizer utilized for training. Although full hyper-parameter optimization can potentially enhance model performance, we opted for a practical approach, exploring a range of learning rates and batch sizes. A learning rate of  $10^{-4}$  is found to provide a good balance between convergence speed and stability. Similarly, a batch size of 64 was chosen as a compromise between computational efficiency and model performance. These settings were sufficient to achieve promising results and demonstrate the effectiveness of our approach.

## 2.3 PID and energy reconstruction

### 2.3.1 The NN prediction

We trained the NNs for three different targets: predicting particle energy, identifying particle type, and jointly predicting both with equal weights. The NN trained to predict particle energy outputs a single numerical value corresponding to the predicted energy. The NN trained for PID produces a multi-class tensor with  $n=4$  values, where  $n$  represents the number of potential incident

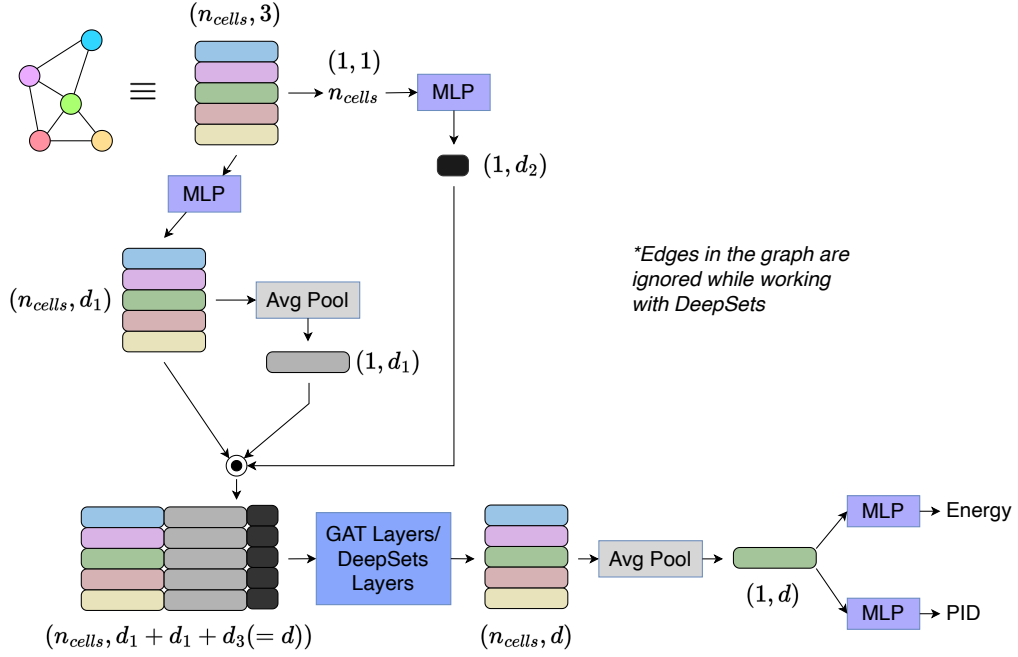


**Figure 4:** The NN architectures. Both the DeepSets and the GAT-based approaches share a similar overall structure, differing only in the use of GAT layers versus DeepSets layers. Since DeepSets does not require edge information, edges are omitted when utilizing this approach. The activated calorimeter cells, coloured circles, represent the point cloud. Each point cloud is independently processed by a MLP to extract the vector of features (coloured ovals) - the node position in space. The feature vectors from all cells are aggregated into a single representation using average Pooling (grey oval). Concatenation is used to combine different feature vectors derived from the input set into a single vector that represents the entire set. After that the set is propagated through GAT/DeepSets layers. The aggregated representation (sage green oval) is further processed by an MLP to generate the final output, either the energy or PID.

particle candidates. These values are normalized using the Softmax function [22] and interpreted as probabilities for each candidate. The particle type is then determined by selecting the candidate with the highest probability. Finally, the NN trained to predict both particle energy and type provides the two outputs.

### 2.3.2 Performance quantification

The energy reconstruction is evaluated by fitting the distribution of  $\frac{\sigma E}{E}$  as a function of the energy of the incoming particle to the commonly used functional form  $\frac{S}{\sqrt{E}} \oplus C$ , where S and C are the stochastic and constant terms, respectively.

To evaluate the PID performance, we used a commonly adopted definition of efficiency in classification tasks. This metric quantifies how accurately the model identifies the target class while avoiding misclassifications. Let Truth Positive (TP) denote the number of events correctly classified as the target class, False Positive (FP) the number of events incorrectly classified as the target class,

and Truth Negative (TN) the number of events correctly classified as not belonging to the target class. The efficiency ( $\varepsilon$ ) and fake rate ( $f$ ) are defined as follows:

$$\varepsilon = \frac{TP}{TP + FP},$$

$$f = \frac{FP}{FP + TN}.$$

The efficiency  $\varepsilon$  measures the proportion of correctly identified target events relative to all instances classified as the target. A high fake rate ( $f$ ) indicates that the model frequently misclassifies non-target events as belonging to the target class. Results are often presented in a so-called confusion matrix in which the rows represent the "True" generated particle and the columns the "Predicted" particle. In this matrix the efficiency values The efficiency  $\varepsilon$  measures the proportion of correctly identified target events relative to all instances classified as the target. A high fake rate ( $f$ ) indicates that the model frequently misclassifies non-target events as belonging to the target class. Results are often presented in a confusion matrix in which the rows represent the "True" generated particle and the columns the "Predicted" particle. In this matrix the diagonal corresponds to the efficiency value and the off-diagonal to the fake rates.

### 3 Results

Each of the two NN architectures was trained to predict one of three targets (only energy, only PID, both energy and PID). The datasets were simulated using the RPWELL-based DHCAL module described in Section 2.1. Four types of hadrons – neutrons, pions, protons, and kaons – were simulated with initial energies uniformly distributed between 1 and 60 GeV. The composition of the training dataset vary to better address the question at hand.

#### 3.1 Particle Identification

The study was carried out assuming 98% Minimum Ionizing Particle (MIP) detection efficiency (as value of choice based on MIP detection efficiency measured with sampling elements of different technologies [4]) and 1.0 average pad-multiplicity for each sampling element. Single neutrons, pions, protons, and kaons were simulated to traverse the center of the DHCAL module perpendicularly to the XY plane (0-degree incidence angle). Four independent datasets, corresponding to each particle type, were combined into a single training dataset comprising 2.4 million events. Additionally, validation and test datasets containing 400k and 440k showers, respectively, were generated with the same composition.

Figure 5 depicts the PID efficiency,  $\varepsilon$ , and fake rate,  $f$ , obtained with a GAT trained to predict only the PID (5a) and with GAT (5b) and DeepSets (5c) trained to predict both PID and the energy at equal weights. An attempt to train DeepSets to predict on the PID failed.

As can be seen in Figure 5, the PID efficiency obtained with all GNNs is close to 100% for protons and kaons and at the level of 80-90% for pions and neutrons where pions are often misidentified as neutrons and vice versa. The strongest identification power was recorded with DeepSets when trained to predict both PID and the energy, in particular the highest efficiency (92%) is achieved for pions.



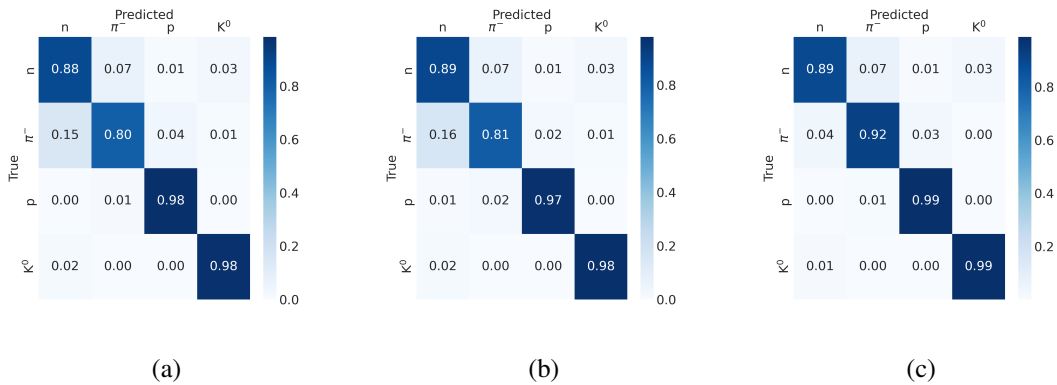


**Figure 5:** PID confusion matrix (see Section 2.3.2) predicted with a GAT trained to predict only the PID (a) and with GAT (b) and DeepSets (c) trained to predict both PID and the energy.

According to [23], the excellent identification of protons and kaons is attributed to baryon and strangeness number conservation, respectively, limiting the production of  $\pi_0$ s in their showers, and hence the event-by-event fluctuations. In contrast, incoming  $\pi^\pm$ s are likely to produce either  $\pi^\pm$ s or  $\pi_0$ s during their interactions.  $\pi_0$ s contribute to an electromagnetic component in the shower. Its magnitude varies significantly depending on the fraction of  $\pi_0$  produced and on the stage at which they are first produced — early or late in the hadronic shower. This impacts both the total measured energy and the shower shape. The poorer PID recorded with neutrons is attributed to large event-by-event fluctuations due to large variety of nuclear interaction - spallation, elastic and inelastic scattering, n-induced fission, etc. - initiating the shower.

Both GAT models misclassified approximately 15% of pions as neutrons. About 95% of these misclassified pions lack the characteristic MIP track, as illustrated in Figure 1(a), at the beginning of their showers. A 4% improvement in pion PID using the GAT (trained to predict only PID) was observed when the proportion of trackless pions in the training dataset was increased from 14% to 29%. This suggests that exposing the model to a wider variety of shower patterns, including those without a distinct MIP track, improves the NN ability to distinguish between pions and neutrons. Additionally, including the total number of clusters in the shower as an input yielded a 2% improvement in the identification of both neutrons and pions.

For the GAT model trained to predict both PID and the energy, changing the weight given to each prediction (0.5-0.5, 0.6-0.4, 0.7-0.3) had negligible effect on the identification performance.

The DeepSets model trained to simultaneously predict both energy and PID, exhibits improved performance with a consistently lower pion fake rate. As depicted in Figure 6, this rate ranges from 6% at lower energies, gradually increasing to 12% at 60 GeV. Neutron mis-classification rates are notably higher for energies below 5 GeV, primarily because at lower energies, the energy deposition patterns of neutrons can closely resemble those of pions, leading to confusion in classification algorithms. The classification efficiencies show minimal dependence on the incident particle energy.

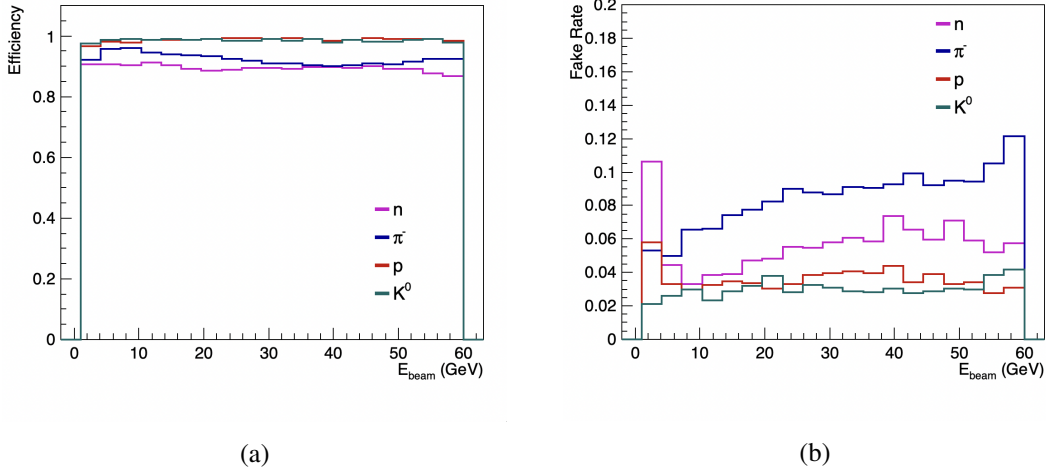


**Figure 6:** The PID efficiency (a) and fake rate (b) as function of the energy of the incoming particle.

### 3.2 Energy reconstruction

For energy reconstruction, negatively charged pions entering the center of the calorimeter perpendicular to its XY plane were studied under various detector response conditions. These include MIP detection efficiencies ranging from 90% to 98%, and average pad multiplicities of 1.0, 1.1, and 1.6. These values align with those reported in previous measurements of RPWELL [4], MicroMegas (MM) [24], and RPC [5] technologies, respectively.

The energy reconstruction performance of DeepSets and GAT models, trained solely to predict energy, is shown in Figure 7. This is compared with traditional algorithms applied to the RPWELL-based DHCAL simulation module [4] and experimental data from the RPC-based CALICE DHCAL [5]. The latter performance was measured up to 32 GeV and extrapolated to 50 GeV in this study. In the low-energy range (up to approximately 15 GeV), DeepSets outperforms all other approaches. Beyond 15 GeV, both DeepSets and GAT demonstrate similar performance, surpassing that of traditional algorithms across the energy range.

DeepSets outperforms GAT in terms of both the stochastic and constant terms, significantly exceeding the required energy resolution of  $55\%/\sqrt{E}$  for future hadron calorimeters. Furthermore, GAT models are considerably more computationally intensive than DeepSets, demanding approximately three times the computational resources and ten times the GPU memory.

To further explore particle-specific performance, four separate DeepSets NNs were trained, each tailored to predict the energy of a distinct hadron type: pion, neutron, kaon, and proton. The resulting energy resolution for each particle, traversing the calorimeter perpendicularly (0-degree incidence angle), is presented in Figure 8.

The energy resolution achieved varies across particle types, with protons and kaons exhibiting significantly better resolution compared to pions and neutrons. This difference is attributed to baryon number conservation in proton showers and strangeness number conservation in kaon induced showers, which reduces event-to-event fluctuations in the production of  $\pi_0$  particles — key carriers of energy in electromagnetic components of hadronic showers. In contrast, the poorer

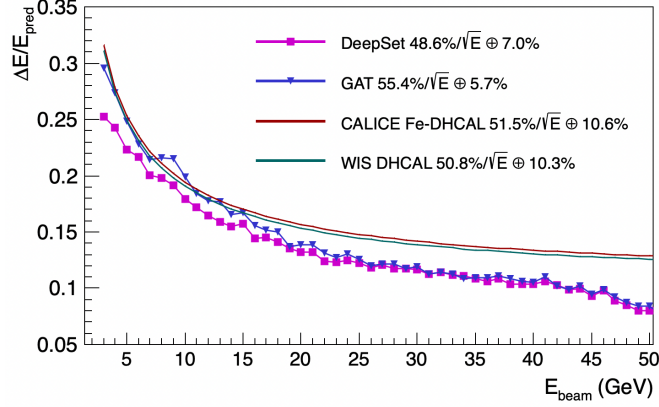


**Figure 7:** The energy resolution predicted by GAT and DeepSets in comparison to that obtained with traditional algorithms employed on the same RPWELL-based DHCAL and CALICE RPC-based DHCAL.

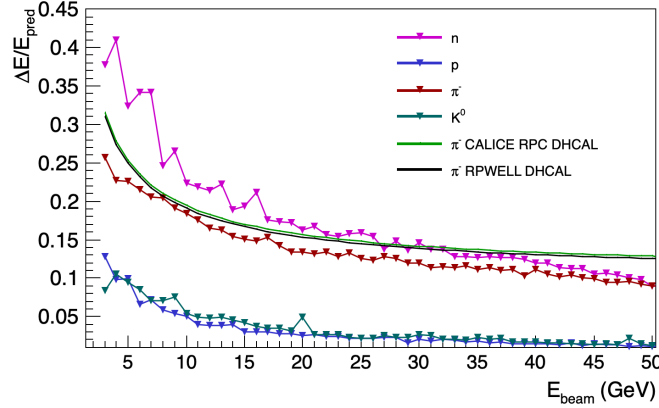


**Figure 8:** The energy resolution of different particles predicted by DeepSets in comparison to that obtained for pions with traditional algorithms employed on the same RPWELL-based DHCAL [4] and CALICE RPC-based DHCAL [5].

resolution observed for neutrons arises from significant event-by-event fluctuations driven by a wide range of nuclear interactions, such as spallation, elastic and inelastic scattering, and neutron-induced fission, which lead to highly variable shower development.

An RPWELL-based DHCAL  $1 \times 1 \text{ m}^2$  module with  $1 \times 1 \text{ cm}^2$  readout elements, assuming a MIP detection efficiency of 98% and an average pad multiplicity of 1, was used to investigate the energy resolution of pions as a function of their incident angle. The variation in shower shape and development with the angle of incidence affects the energy deposition patterns within the DHCAL, potentially affecting the measured resolution.

The influence of the incident angle on energy reconstruction was investigated using two training datasets, each containing 1.8 million simulated pion showers. These datasets were generated with

pion energies uniformly distributed between 1 and 60 GeV and angles uniformly sampled within  $0^\circ-10^\circ$ ,  $0^\circ-20^\circ$ , as illustrated in Figure 9. Comparison of these two datasets revealed no significant degradation in energy resolution up to an incident angle of  $20^\circ$ . Beyond this angle, however, a decrease in resolution is anticipated due to the increased diversity of shower shapes and energy deposition profiles, coupled with enhanced lateral shower leakage from the calorimeter. We plan to expand and potentially refine the training datasets and conduct further studies that incorporate the prediction of the incident angle alongside energy reconstruction.

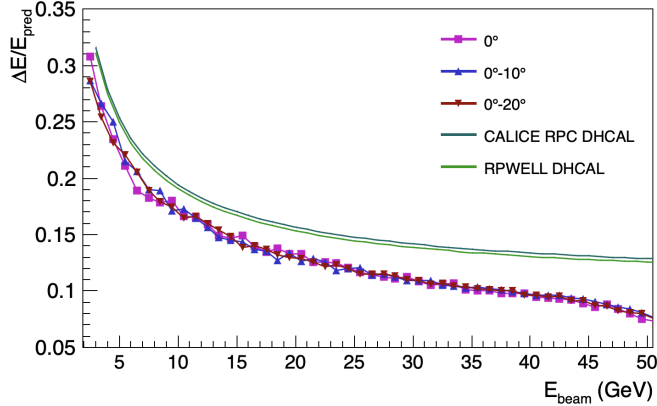


**Figure 9:** The energy resolution of pions predicted by DeepSets trained over different ranges of incoming particles angles.

### 3.3 Different detector performance and design

We investigated the sensitivity of GNNs models to various DHCAL detector parameters, including pad size, pad multiplicity, and MIP detection efficiency. Pion training and testing datasets were generated for various readout granularity and detector performances as shown in Table 1.

Module	$\varepsilon_{MIP}$	multiplicity	pad size
$M_{RPWELL}$ [4]	98%	1.1	$1 \times 1 \text{ cm}^2$
$M_2$	98%	1.1	$2 \times 2 \text{ cm}^2$
$M_3$	98%	1.1	$3 \times 3 \text{ cm}^2$
$M_4$	98%	1.1	$4 \times 4 \text{ cm}^2$
$M_5$	95%	1.1	$1 \times 1 \text{ cm}^2$
$M_6$	90%	1.1	$1 \times 1 \text{ cm}^2$
$M_{RPC}$ [5]	96%	1.6	$1 \times 1 \text{ cm}^2$

**Table 1:** List of simulated modules.  $M_{RPWELL}$  and  $M_{RPC}$  correspond to the RPWELL-based DHCAL and CALICE-Fe-DHCAL performance studied in [4] and [5], respectively.

The baseline design of DHCAL module is pad size of  $1 \times 1 \text{ cm}^2$ . The dependency of the pion energy resolution for various pad sizes is shown in Figure 10a. It demonstrates that enlarging the

pad's size by a factor of four ( $2 \times 2 \text{ cm}^2$ ) and correspondingly reducing the number of channels by four does not degrade the performance significantly. Provided that the two shower separation would not degrade as well, these may offer more cost-effective solution for future experiments. Additionally, the model demonstrated robustness to variations in MIP detection efficiency, as illustrated in Figure 10b. The detector modules simulated with lower MIP efficiencies — the M5 and M6 modules with efficiencies of 90% and 95%, respectively — do not significantly impact the resolution. This allows for less stringent restrictions on gain settings, facilitating improved performance without compromising the overall detection capabilities.

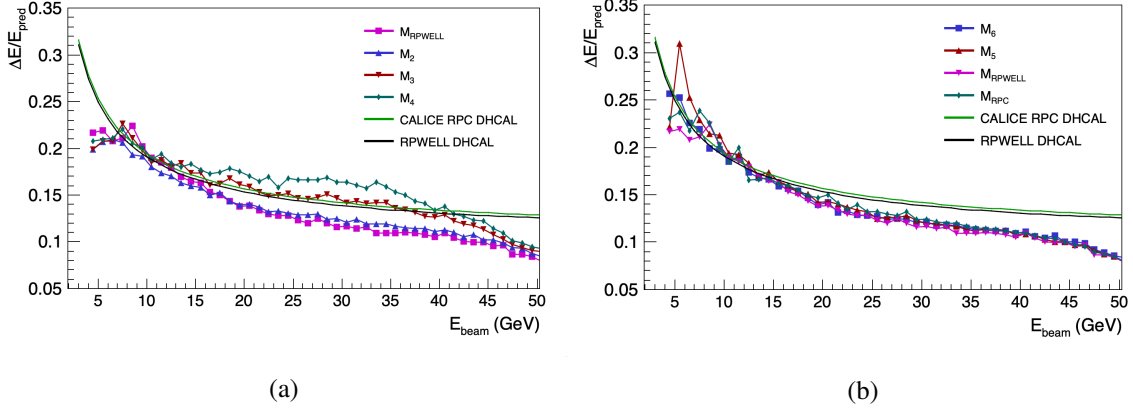


**Figure 10:** (a) The energy resolution of pion predicted by DeepSets for different readout pad sizes. (b) The energy resolution of pions predicted by GAT for varying MIP detection efficiencies and average pad multiplicities.

## 4 Discussion

We investigate potential improvements in the design and performance of future DHCAL systems using GNN algorithms. These algorithms exploit the representation of hadronic showers as point clouds or connected graphs, offering a more detailed analysis of the shower structure. Multiple DeepSet and GAT architectures were trained to predict two objectives — either separately or in combination: the energy and type of the incoming particle. The performance of these NNs was compared both to each other and to traditional reconstruction algorithms, which primarily rely on counting the number of hits and re-weighting them based on their density. Unlike GNN-based approaches, traditional methods do not fully leverage the detailed spatial and structural information of the shower shape.

Training DeepSet to predict the PID and energy together, a PID at the level of 90% was recorded for pions and neutrons and approximately 100% for proton and kaons. This performance surpasses that of GAT trained for the same target and the two NNs trained solely to predict the PID. Across all particle types, the efficiency showed minimal dependence on particle energy. However, a somewhat stronger energy dependence was observed in the fake rates of pions and neutrons.

Compared to standard energy reconstruction algorithms, all tested NNs demonstrated improved pion energy resolution, with the best performance achieved across the entire energy range by the

DeepSets model trained exclusively for energy prediction; stochastic term of 48.6% and constant term of 7%. The recorded energy resolution of neutrons and pions was found significantly poorer than that of protons and kaons.

The poorer performance recorded with pions and neutrons relative to protons and kaons for both of PID and energy reconstruction is in agreement with models discussing fluctuations in the shape of these particles showers. Further research is needed to improve the energy resolution for pions and neutrons, through the investigation of the impact of different training strategies and network architectures that could lead to enhancements in the model's accuracy and robustness.

The relatively poorer performance observed with pions and neutrons, compared to protons and kaons, in both PID and energy reconstruction is consistent with phenomenological models that attribute the disparity to fluctuations in the shapes of their particle showers. Addressing this challenge requires further research aimed at improving the performance of pions and neutrons, e.g., enhancing the training dataset with low energy neutrons or with trackless pions to better distinguish them from neutrons.

DeepSets was trained on datasets featuring pion showers with a uniform range of incoming particle angles to evaluate the impact of angle variation on energy resolution. A performance degradation was observed when the NN was trained on a broader angular range ( $0^\circ$ – $30^\circ$ ). This degradation is likely due to the increased diversity of shower shapes at each energy, which could be partially mitigated by expanding the size of the training dataset. Further studies to resolve this degradation are ongoing.

In terms of pion energy resolution, a DHCAL module with a pad size of  $2 \times 2 \text{ cm}^2$  performs as good as a module featuring a pad size of  $1 \times 1 \text{ cm}^2$ . Furthermore, the energy resolution achieved using the DeepSets algorithm on showers recorded with a DHCAL module with a  $3 \times 3 \text{ cm}^2$  pad size was comparable to that obtained using traditional algorithms applied to data from a module with  $1 \times 1 \text{ cm}^2$  pads. These results suggest that simpler and more cost-effective DHCAL designs, with one-fourth or even lower granularity, could suffice for future experiments without compromising performance. Only a minor dependency of the pion energy resolution on the MIP detection efficiency and average pad multiplicity was found, potentially posing weaker requirements on the performance of the sampling elements in future DHCAL systems. Future studies on two-track separation, overall jet-energy resolution, and off-axis showers are crucial for such future decision making.

## Acknowledgments

This study is supported by the Minerva Foundation with funding from the Federal German Ministry for Education and Research, as well as by the Kreter-Perinot Center for High-Energy Particle Physics. Additional support comes from a research grant provided by Shimon and Golde Picker, the Nella and Leon Benozziyo Center for High Energy Physics, and the Sir Charles Clore Prize. Special thanks go to Martin Kushner Schnur for his invaluable support of this research.

## References

- [1] M.A. Thomson, *Particle Flow Calorimetry and the PandoraPFA Algorithm*, *Nucl. Instrum. Meth. A* **611** (2009) 25 [0907.3577].

- [2] R. Wigmans, *Calorimetry*, Oxford Science Publications (2000).
- [3] CMS, CALICE collaboration, *Performance of the CMS High Granularity Calorimeter prototype to charged pion beams of 20–300 GeV/c*, *JINST* **18** (2023) P08014 [2211.04740].
- [4] D. Shaked-Renous et al., *Test-beam and simulation studies towards RPWELL-based DHCAL*, *JINST* **17** (2022) P12008 [2208.12846].
- [5] CALICE collaboration, *Analysis of Testbeam Data of the Highly Granular RPC-Steel CALICE Digital Hadron Calorimeter and Validation of Geant4 Monte Carlo Models*, *Nucl. Instrum. Meth. A* **939** (2019) 89 [1901.08818].
- [6] F.A. Di Bello, S. Ganguly, E. Gross, M. Kado, M. Pitt, L. Santi et al., *Towards a Computer Vision Particle Flow*, *Eur. Phys. J. C* **81** (2021) 107 [2003.08863].
- [7] J. Pata, E. Wulff, F. Mokhtar, D. Southwick, M. Zhang, M. Girone et al., *Improved particle-flow event reconstruction with scalable neural networks for current and future particle detectors*, *Commun. Phys.* **7** (2024) 124 [2309.06782].
- [8] CMS collaboration, *Deep learning techniques for energy clustering in the CMS electromagnetic calorimeter*, *Nucl. Instrum. Meth. A* **1049** (2023) 168082.
- [9] CMS HGCAL collaboration, *Timing Performance of the CMS High Granularity Calorimeter Prototype*, *JINST* **19** (2024) P04015 [2312.14622].
- [10] F.A. Di Bello et al., *Reconstructing particles in jets using set transformer and hypergraph prediction networks*, *Eur. Phys. J. C* **83** (2023) 596 [2212.01328].
- [11] CALICE collaboration, *Software Compensation for Highly Granular Calorimeters using Machine Learning*, *JINST* **19** (2024) P04037 [2403.04632].
- [12] CMS HGCAL, CALICE AHCAL collaboration, *Using graph neural networks to reconstruct charged pion showers in the CMS High Granularity Calorimeter*, *JINST* **19** (2024) P11025 [2406.11937].
- [13] S. Song, J. Chen, J. Liu, Y. Liu, B. Qi, Y. Shi et al., *Study of residual artificial neural network for particle identification in the CEPC high-granularity calorimeter prototype*, *JINST* **19** (2024) P04033 [2310.09489].
- [14] B. Liu, I. Laktineh, Q. Shen, G. Garillot, J. Guo, F. Lagarde et al., *Particle identification using Boosted Decision Trees in the semi-digital hadronic calorimeter*, *JINST* **15** (2020) C05022.
- [15] GEANT4 collaboration, *GEANT4—a simulation toolkit*, *Nucl. Instrum. Meth. A* **506** (2003) 250.
- [16] J. Shlomi, P. Battaglia and J.-R. Vlimant, *Graph neural networks in particle physics*, *Machine Learning: Science and Technology* **2** (2020) 021001.
- [17] M. Zaheer, S. Kottur, S. Ravanbakhsh, B. Póczos, R. Salakhutdinov and A. Smola, *Deep Sets*, 2018.
- [18] J. Yuan, S. Chen, Y. Zhang, Z. Shi, X. Geng, J. Fan et al., “Graph attention transformer network for multi-label image classification.” arXiv:2203.04049, 2024.
- [19] A. Vaswani, N. Shazeer, N. Parmar, J. Uszkoreit, L. Jones, A.N. Gomez et al., “Attention is all you need.” arXiv:1706.03762, 2023.
- [20] A. Paszke et al., *Automatic differentiation in PyTorch*, in *NIPS 2017 Workshop Autodiff*, 2017, <https://openreview.net/forum?id=BJJsrnfCZ>.
- [21] Ilya Loshchilov and Frank Hutter, *Decoupled Weight Decay Regularization*, in *International Conference on Learning Representations*, 2017, <https://api.semanticscholar.org/CorpusID:53592270>.

- [22] G.O. Y. LeCun, L. Bottou and K.-R. Müller, *Efficient backprop*, in *Neural networks: Tricks of the trade*, Springer (2002).
- [23] N. Akchurin et al., *On the differences between high-energy proton and pion showers and their signals in a non-compensating calorimeter*, *Nucl. Instrum. Meth. A* **408** (1998) 380.
- [24] C. Adloff et al., *Construction and test of a 1x1m<sup>2</sup> Micromegas chamber for sampling hadron calorimetry at future lepton colliders*, *Nucl. Instrum. Meth. A* **729** (2013) 90.